Optical scanning of laser line sensors for 3D imaging

Johannes Schlarp[1*], Ernst Csencsics[1], and Georg Schitter[1]

[1] *Christian Doppler Laboratory for Precision Engineering an Automated In-Line Metrology, Automation and Control Institute (ACIN), TU Wien, 1040 Vienna, Austria*
[*] *Corresponding author: schlarp@acin.tuwien.ac.at*

Compiled January 28, 2020

In scanning laser triangulation sensors for 3D imaging the achievable throughput is strongly limited by the moving mass. By realizing an optical scanning approach rather than repositioning the entire sensor, this limitation could be reduced, leading to a reduced measurement time. This work presents sensor system geometries in which only the optical path of a line triangulation sensor is manipulated by a tip-tilt mirror. In the proposed rotational scanning systems either the illumination path, or both the illumination and the reflection path are manipulated. By using ray-tracing simulation the performance of the scanning systems are optimized and possible disadvantages can be determined up front. Using geometric relations, the surface profile can be reconstructed from the measured sensor data, the mirror position and the model parameters. Experimental results show that the image quality of the proposed rotational scanning systems is comparable to systems based on classical translational scanning motion.

OCIS codes: (150.6910) Three-dimensional sensing, (150.3045) Industrial optical metrology, (120.4880) Optomechanics, (280.3420) Laser sensors, (230.4040) Mirrors, (280.4788) Optical sensing and sensors

http://dx.doi.org/10.1364/ao.XX.XXXXXX

1. INTRODUCTION

In recent years, optical three-dimensional measurement systems have become increasingly relevant for the quality assurance of production processes [1–5]. Due to the optical measurement principles, high resolutions and short measurement times can be achieved [6]. For example, camera-based three-dimensional image sensors, which obtain the surface profile directly from the sample, can be used [7]. These sensors use active or passive light sources for illumination and cameras to capture the sample. From the known geometric relations and the captured image, the surface profile of the sample can be obtained. However, in such systems the achievable resolution is limited [2]. For example phase-shift fringe projection systems are a frequently used camera-based sensor and achieve resolutions up to 10 μm [7].

An approach to obtain three-dimensional data with higher resolution is to combine point or line sensors with external actuators, such as linear stages [8, 9], coordinate measurement machines [10] or industrial robots [11]. With the external actuator the position of the entire sensor (Fig. 1(a)) or the sample is manipulated [12]. The positioning bandwidth of the actuator determines, among other parameters, the achievable measurement time. If optical sensors are used, it is also possible to manipulate only the optical path (Fig. 1(b)) to create a scanning motion. Since the moving mass of a scanning mirror system is lower as compared to a classical translational scanning system with the entire sensor, the measurement time can be reduced [13]. In addition, the rotational scanning system can be realized in a compact unit, making it easier to integrate it in a measurement application.

In [14] a scanning confocal sensor, which manipulates the optical path of a confocal sensor with a galvanometer mirror, is presented. With a varifocal liquid lens, which changes the focal length according to the applied voltage, the laser spot is focused on the sample. A scanning triangulation sensor system, which incorporates two galvanometer mirrors to manipulate the position of the laser spot, is presented in [2]. Additional fixed mirrors are used to redirect the beams between the two galvanometers, which leads to a rather complex system design. In [15, 16] basic ideas for scanning triangulation sensor system are shown. In these designs only the illumination path of the sensor is manipulated by a mirror. Furthermore, the achievable accuracy of the scanning system is estimated for various scan ranges.

Laser triangulation sensors are frequently used non-contact measurement systems in quality control and dimensional metrology, due to their high resolution and large measurement range [9]. With this sensors resolutions up to 30 nm can be accomplished, which is significantly smaller compared to camera-based sensors like phase-shift fringe projection systems [17]. Triangulation sensors typically consist of a laser diode to generate a laser beam, that is focused on the sample, where light is scattered at the point where the beam irradiates the sample.

Post-print version of the article: J. Schlarp, E. Csencsics, and G. Schitter, "Optical scanning of laser line sensors for 3D imaging", *Applied optics*, vol. 57, no. 18, pp. 5242–5248, 2018. DOI: 10.1364/AO.57.005242

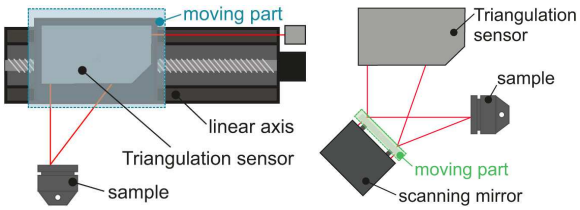

(a) Translational scan (b) Rotational scan

Fig. 1. In conventional systems the sensor (a) or the sample is moved by an actuator, to obtain the surface profile of the sample. The achievable measurement time is limited by the large moving mass. By manipulating only the optical path (b) of an optical sensor, this limitation can be reduced.

With a lens, the scattered light is projected onto the detector. The lateral position of the projected point provides an accurate measure of the distance between the sensor and the sample. Triangulation sensors for industrial applications are available as point and line sensors, with different measurement ranges from 1 mm up to 1000 mm [7].

In many scanning systems galvanometers or rotating polygons are used as fast scanners [18, 19], which suffer from poor linearity during fast linear scanning and large rotational moment of inertia [20]. With MEMS scanners large deflection angles as well as high resonance frequencies can be achieved, but their small aperture size limits their application in scanning systems [21]. Fast steering mirrors (FSMs), e.g. for tip and tilt motion, offer advantages such as fast response and small rotational moment of inertia [20]. Due to their compact design, it is possible to integrate them into a compact scanning system [22]. Depending on the application either a high bandwidth or a large scan range is required, which are realized by piezoelectric [23] or electromagnetic actuators [24, 25].

The contribution of this paper is the investigation of optical scanning triangulation systems, which achieve a comparable image quality with lower moving masses compared to a classical translational scanning system. In Section 2 the system architectures of two scanning laser line sensors are presented. In the first proposed scanning system only the illumination path of the laser line sensor is manipulated, while the second scanning system manipulates both optical paths of the sensor by means of an FSM. The experimental setups are presented in Section 3, followed by the validation of the measurement results in Section 4. Section 5 concludes the paper.

2. SYSTEM DESIGN

A. System architecture

For the optical scanning system either a point or a line triangulation sensor can be used. In this paper the optical path of the line sensor is manipulated only in one direction with the tip-tilt mirror to obtain the surface profile of the sample. Two specific realizations are proposed and investigated: (i) either scanning the illumination path only, or (ii) scanning both optical paths of the line sensor by the tip-tilt mirror (see Fig. 2).

In Fig. 2(a) the system architecture of the scanned illumination path system (SIS) is shown for different lateral positions of the measurement line on the sample. In order to project the diffusely reflected light of the laser line on the detector, the sample must be located in front of the sensor. Therefore, the illumination path is deflected not only by the tip-tilt mirror but also by a static mirror (Fig. 2(a)). By rotating the tip-tilt mirror around its x-axis the position of the laser line on the sample, which is parallel to the x-axis, is varied along the y-axis. The closer the tip-tilt mirror is mounted to the sensor, the larger is the achievable lateral scan range. Since the laser line expands in x-direction during the propagation, the required aperture size increases for both mirrors with the distance between sensor and the respective mirror. The achievable scan speed of the tip-tilt mirror is decreasing as the aperture size increases [26]. As a result, the tip-tilt mirror should be mounted close to the sensor, such that a small and fast tip-tilt mirror can be used. The triangulation sensor acquires the distance between sample and sensor along the z-plane, shown in Fig. 2(a) (blue dots). It is also notable, that the position of the laser line on the detector changes strongly for different lateral positions, such that a large measurement range is required to scan a flat surface. This yields to a limitation in the scan process, since extended objects can not be detected over the entire lateral scan range.

The system architecture of the scanned illumination and reflection path system (SIRS) is depicted in Fig. 2(b) for different lateral positions of the measurement line on the sample. In this setup both optical paths of the laser line sensor are scanned along the y-direction by the tip-tilt mirror. The achievable lateral scan range of this system architecture again depends on the distance between sensor and tip-tilt mirror. However, the required aperture size increases when the tip-tilt mirror is positioned closer to the sensor, as both paths need to be redirected. Therefore, a tradeoff between lateral scan range and achievable bandwidth need to be made. Since the roughness of the mirror surface is small as compared to the wavelength of the laser beam, there is no difference from the perspective of the sensor, if the entire optical path is manipulated by the tip-tilt mirror. The laser triangulation sensor measures the total length of the illumination beam. This length changes only slightly during the scan of a flat surface, shown in Fig. 2(b), such that the required range for measuring a flat surface is significantly smaller.

B. Simulation

To evaluate the two system architectures of the scanning system in advance, ray-tracing simulations are performed. This allows an easy and fast way to compare the system geometries with each other. Thereby, the crucial parameters of the system, such as the achievable measurement range, errors due to poor alignment or aberrations can be estimated up front. For the simulation the positions and properties of the individual optical components are specified initially. Subsequently the simulation program (Matlab, Mathworks, Natick, USA) calculates and displays the resulting optical path.

The chosen system architectures are based on a laser line sensor (Type: scanCONTROL 2660-100, Micro-Epsilon GmbH, Germany) with a measurement range of 100 mm. The first evaluated architecture is the SIS, shown in Fig. 2(a). In order to avoid additional lateral shifts which are induced by an offset to the pivot point, the laser line hits the mirror surface in the center. Since the illumination path of the SIS is manipulated close to the sensor, a tip-tilt mirror with a small aperture size (32 mm) can be used, enabling a higher scanning speed [26]. As described earlier, the measured distance between the sensor and the sample is acquired along the z-plane (see Fig. 2(a)). Since the emergent angle θ of the reflected laser line is small (between 12.73° and 14.18°), a large measurement range is required to

Post-print version of the article: J. Schlarp, E. Csencsics, and G. Schitter, "Optical scanning of laser line sensors for 3D imaging", *Applied optics*, vol. 57, no. 18, pp. 5242–5248, 2018. DOI: 10.1364/AO.57.005242

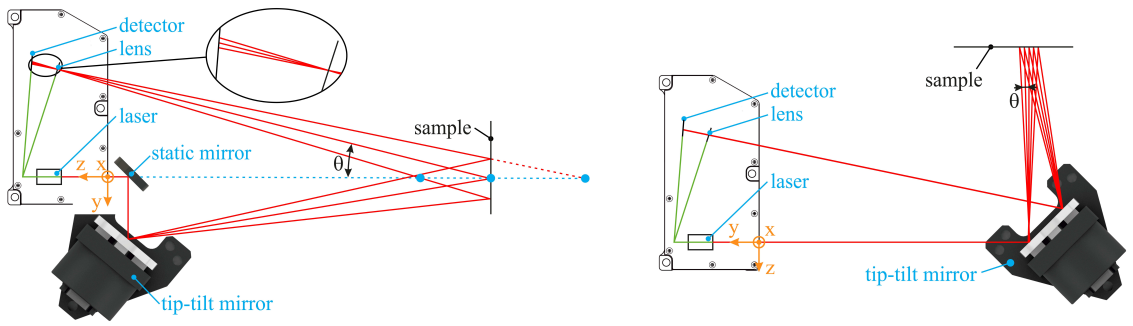

(a) Scanned illumination path system (SIS)

(b) Scanned illumination and reflection path system (SIRS)

Fig. 2. System architectures of an optical scanning system. Either only the illumination path (a) or both optical paths (b) of the laser line sensor are manipulated by the tip-tilt mirror. The sensor laser line is in both cases parallel to the x-axis.

scan a flat surface. Fig. 3 shows a simulation of measured sensor values as a function of the lateral position of the scan line on a flat sample. The measured flat surface is positioned in the middle of the measurement rang of the sensor (at 50 mm). For the SIS the selected sensor, with a measurement range of 100 mm, can only accomplish a lateral scanning range of 26.6 mm. This leads to a limitation in the scan process, since extended objects, which are located at the margins of the scan area can not be detected. Besides the measurement range and the alignment of the separate components, the actuation range of the tip-tilt mirror determines the achievable lateral scan range. With the other parameters determined and a selected lateral scan range of 25 mm, an actuation range of the tip-tilt mirror of $\pm 1.5°$ is required.

In Fig. 2(b) the SIRS architecture, in which both optical paths are manipulated, is shown. As described earlier, this architecture requires a tradeoff between lateral scan range and achievable bandwidth. For better comparison of the measurement results from the two rotational scanning systems, the same tip-tilt mirror is used in both system architectures. As a result, a tip-tilt mirror with an aperture size of two inches and an actuation range of $\pm 1.5°$ is used. The resulting achievable lateral scan range of the SIRS is 10.2 mm, which is smaller compared to the proposed SIS. As shown in Fig. 3, the required sensor range for a lateral scan of a flat surface can, however, be reduced by a factor of 95.95% in comparison to the SIS. Therefore, the limitation in the scan process for extended objects, which occur at the SIS, can be almost completely eliminated for the SIRS.

In Fig. 2(b) it is notable, that the position of the laser line on the detector is alike for different lateral positions. This can be attributed to the fact, that the measured distance in the SIRS only increases by the factor $1/\cos(\theta)$ during the scan motion. For the SIS the position of the laser line on the detector changes strongly for different lateral positions, which can be noticed in the zoomed image in Fig. 2(a).

C. Geometrical relations for data reconstruction

In conventional 3D measurement systems that incorporate point or line sensors, the sensor or the sample is typically moved by external position controlled actuators, that may be aligned with the surface under test. From the measured distance between sensor and sample, and the position of the actuators, the surface profile of the sample can be directly reconstructed [10]. Thereby,

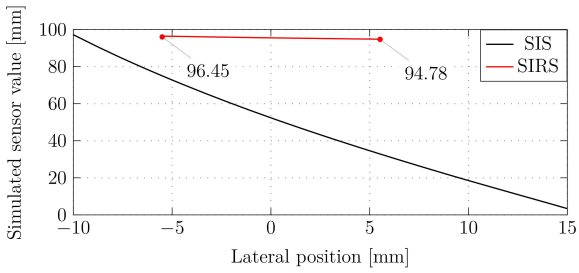

Fig. 3. Simulation of the required sensor range to scan a flat surface with the SIS and SIRS. For the SIS almost the entire sensor range of the sensor (100 mm) is required to scan a lateral range of 26.6 mm. Due to the change of both optical paths in the SIRS, the required measurement range can be reduced by 95.95%.

the surface profile is described by the, in this case directly measured, absolute values x_l, y_l and z_l. For the proposed scanning laser line sensors the measured quantities include the values x_{meas}, z_{meas} which are acquired by the laser line sensor along the x- and z-axis and the angular position $\Delta\varphi$ of the tip-tilt mirror. With this measured quantities the profile can not be directly obtained. Therefore, the geometric relations between the measured and absolute values have to be determined.

The calculation of the SIS is based on the schematic setup shown in Fig. 4. In order to obtain the geometrical relations needed for reconstruction of the surface profile from the measured quantities, the similarity theorems for triangles as well as trigonometric functions are required [27]. With the shown triangles (dash-dotted line, blue and green) in the schematic setup, the relation between the measured distance z_{meas} and the absolute value z_l can be expressed by

$$\frac{z_{meas} + z_{lens}}{y_{lens}} = \frac{z_l + z_{lens}}{y_{lens} + y_l}, \tag{1}$$

with the position of the lens y_{lens} and z_{lens}. This position is generally not specified by the manufacturer, but it can be estimated with the beam path of the sensor, shown in the dimensional drawing [28], and the least squares method [29]. The absolute

Post-print version of the article: J. Schlarp, E. Csencsics, and G. Schitter, "Optical scanning of laser line sensors for 3D imaging", *Applied optics*, vol. 57, no. 18, pp. 5242–5248, 2018. DOI: 10.1364/AO.57.005242

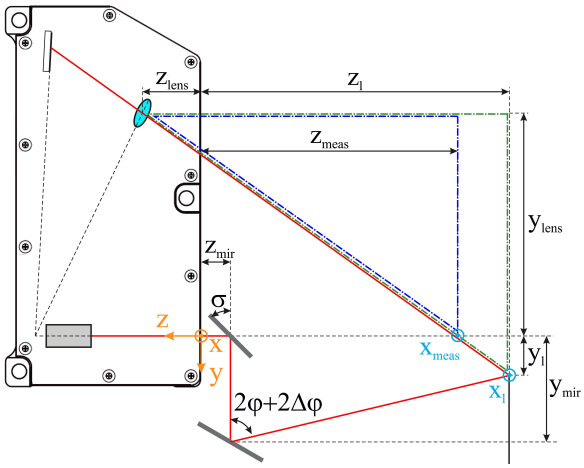

Fig. 4. Schematic setup of the SIS. In order to reconstruct the surface profile from the measured quantities and the model parameters, the similarity of triangles (dash-dotted line, blue and green) as well as the trigonometric functions are used.

value y_l can be calculated with the trigonometric functions

$$\tan(2\varphi + 2\Delta\varphi) = \frac{(z_l - z_{mir})}{(y_{mir} - y_l)}, \tag{2}$$

for $\sigma = 45°$. The parameters y_{mir}, z_{mir} and φ specify the position and orientation of the tip-tilt mirror, with respect to the laser line sensor. Since the value x_{meas} is also determined along the z-plane (Fig. 4), the absolute value x_l has to be calculated with the similarity theorems for triangles and can be expressed by

$$\frac{z_{meas}}{x_{meas}} = \frac{z_l}{x_l}. \tag{3}$$

To calculate the surface profile of the sample the Eqn. (1)-(3) can be rearranged in the following form

$$y_l = \frac{y_{lens}[\tan(2\varphi + 2\Delta\varphi)y_{mir} - z_{meas} - z_{mir}]}{y_{lens}\tan(2\varphi + 2\Delta\varphi) - z_{meas} + z_{lens}} \tag{4a}$$

$$z_l = z_{meas}\left(1 + \frac{y_l}{y_{lens}}\right) + z_{lens}\frac{y_l}{y_{lens}} \tag{4b}$$

$$x_l = x_{meas}\frac{z_l}{z_{meas}}, \tag{4c}$$

with the model parameters according to Table 1.

Table 1. Calculated parameters of the SIS.

Parameter	Value	Parameter	Value
φ	41.7°	z_{mir}	13.2 mm
σ	45°	y_{lens}	73.18 mm
y_{mir}	41.7 mm	z_{lens}	37.15 mm

Fig. 5 shows the schematic setup of the SIRS and is used to determine the geometric relations. Since the laser line of the illumination path does not hit the center of the tip-tilt mirror, an

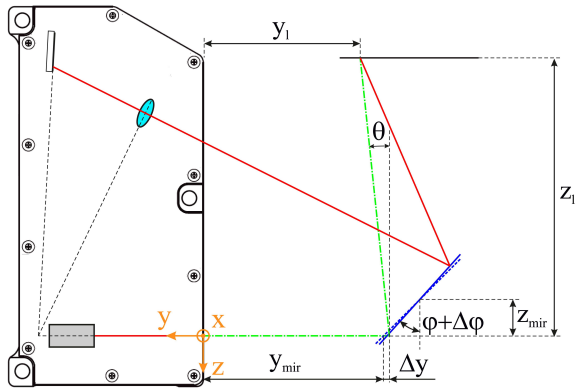

Fig. 5. Schematic setup of the SIRS. To reconstruct the surface profile out of the measurement data, the lateral displacement Δy of the mirror surface has to be considered. The measured size z_{meas} is represented by the total length of the dashed-dotted line (green).

additional translational displacement of the mirror surface in the y-direction occurs, where Δy can be considered by

$$\Delta y = z_{mir}[\tan(\varphi) - \tan(\varphi + \Delta\varphi)]. \tag{5}$$

For the calculation of the absolute values, the angle of the laser beam θ is required. This angle can be calculated using the law of reflection [30], which yields

$$\theta = 90° - 2\varphi - 2\Delta\varphi. \tag{6}$$

The geometrical relations for the SIRS can be derived with trigonometric functions

$$y_l = [z_{meas} - y_{mir} - \Delta y]\sin(\theta) - y_{mir} - \Delta y \tag{7a}$$

$$z_l = -[z_{meas} - y_{mir} - \Delta y]\cos(\theta) \tag{7b}$$

$$x_l = x_{meas}, \tag{7c}$$

in which z_{meas} represents the total beam length of the illumination path (dash-dotted line, green). As described earlier, for the SIRS there is no difference from the perspective of the sensor, if the optical path is manipulated by the tip-tilt mirror. Therefore, the measured value x_{meas} corresponds to the absolute value x_l.

An advantage of this setup is, that for the data reconstruction the lens position is not required. For this reason it is not shown in Table 2, where the chosen model parameters for the SIRS are listed.

Table 2. Calculated parameters of the SIRS.

Parameter	Value	Parameter	Value
y_{mir}	180 mm	φ	45°
z_{mir}	12 mm		

3. EXPERIMENTAL SETUPS

In order to verify the results of the laser scanning systems by reference measurements of the chosen samples, the laser line sensor

Post-print version of the article: J. Schlarp, E. Csencsics, and G. Schitter, "Optical scanning of laser line sensors for 3D imaging", *Applied optics*, vol. 57, no. 18, pp. 5242–5248, 2018. DOI: 10.1364/AO.57.005242

is mounted on a position controlled linear stage (Type: VT-80 62309160, Physik Instrumente GmbH, Germany), as shown in Fig. 6(a). At the end position of the controlled linear stage the optical path is manipulated by the static mirror (Type: PF10-03-F01, Thorlabs, Inc., New Jersey, USA) and the tip-tilt mirror (Type: OIM102, Optics In Motion LLC, Long Beach, USA). These components are aligned according to the ray-tracing simulation and the model parameters (Table 1). With a manual linear stage the tip-tilt mirror is arranged. To synchronize the measured data of the triangulation sensor with the position data of the tip-tilt mirror the integrated synchronization input of the laser line sensor is used.

In Table 3 the achievable maximum measurement range as well as the resolutions of the proposed SIS are listed. Due to the actuation range of the tip-tilt mirror ($\pm 1.5°$) the achievable scan range in the y-direction is limited. However, the achievable bandwidth decreases if a mirror with a larger actuation range is used [26]. Therefore, a tradeoff between lateral scan range and achievable bandwidth need to be made. The resolution in x- and z-direction is determined by the laser line sensor itself, while in y-direction the resolution is strongly affected by the angular resolution φ_{res} of the tip-tilt mirror. By adapting Eqn. 4a the resolution can be determined to

$$y_l(\Delta\varphi, \varphi_{res}) = \frac{y_{lens}[\tan(2\varphi + 2\Delta\varphi + 2\varphi_{res})y_{mir} - z_{max} - z_{mir}]}{y_{lens}\tan(2\varphi + 2\Delta\varphi + 2\varphi_{res}) - z_{max} + z_{lens}} \quad \textbf{(8a)}$$

$$y_{res} = \max_{\Delta\varphi_{min} \leq \Delta\varphi \leq \Delta\varphi_{max}} |y_l(\Delta\varphi, \varphi_{res}) - y_l(\Delta\varphi, 0)| \quad \textbf{(8b)}$$

with $\Delta\varphi_{min}$ and $\Delta\varphi_{max}$ the minimal and maximal angular position and z_{max} the maximal measurement distance of the laser line sensor.

Table 3. Achievable scan range and resolution of the SIS.

Parameter	Value	Parameter	Value
Δx_{meas}	120.8 mm	x_{res}	188.75 μm
Δy_{meas}	24.4 mm	y_{res}	122.9 μm
Δz_{meas}	100 mm	z_{res}	200 μm

Fig. 6(b) shows the experimental setup of the SIRS. With a manual linear stage the tip-tilt mirror is aligned, according to the chosen model parameters given in Table 2. For the rotational scans the controlled linear stage is moved to the end position. Due to the aperture size and circular shape, not the complete laser line can be reflected along the x-axis by the mirror surface. Therefore, the achievable measurement range in x-direction, shown in Table 4, is decreased compared to the SIS. Because of the large distance between the sensor and the tip-tilt mirror, the measurement range starts shortly after the mirror surface, such that the measurement range in the z-direction is decreased by 14 mm. If a larger aperture size is used, the mirror could be positioned closer to the sensor, such that the achievable measurement range could be expand in all directions. However, this would also increase the moving mass, resulting in a lower scan speed. The resolution in x- and z-direction is similar to the SIS, to calculate the resolution in y-direction, which is again determined by the angular resolution of the mirror, the Eqn. 5-7a need to be modified to

$$\Delta y(\Delta\varphi, \varphi_{res}) = z_{mir}[\tan(\varphi) - \tan(\varphi + \Delta\varphi + \varphi_{res})] \quad \textbf{(9a)}$$

$$\theta(\Delta\varphi, \varphi_{res}) = 90° - 2\varphi - 2\Delta\varphi - 2\varphi_{res} \quad \textbf{(9b)}$$

$$y_l(\Delta\varphi, \varphi_{res}) = [z_{max} - y_{mir} - \Delta y(\Delta\varphi, \varphi_{res})]\sin(\theta(\Delta\varphi, \varphi_{res})) - y_{mir} - \Delta y(\Delta\varphi, \varphi_{res}) \quad \textbf{(9c)}$$

$$y_{res} = \max_{\Delta\varphi_{min} \leq \Delta\varphi \leq \Delta\varphi_{max}} |y_l(\Delta\varphi, \varphi_{res}) - y_l(\Delta\varphi, 0)|. \quad \textbf{(9d)}$$

Table 4. Achievable scan range and resolution of the SIRS.

Parameter	Value	Parameter	Value
Δx_{meas}	40 mm	x_{res}	188.75 μm
Δy_{meas}	10.2 mm	y_{res}	51.3 μm
Δz_{meas}	86 mm	z_{res}	200 μm

4. VALIDATION OF THE MEASUREMENT RESULTS

To validate the scanning laser line sensors the measurement results are compared to the reference measurement. Different samples are used to cover a wide range of applications. However, the results of the various sample are similar, such that only the measurement results of the memory chips of a graphic card are depicted. In Fig. 7 the results of the SIS are shown. To compare the reference measurement with the rotational scan quantitatively a RANSAC algorithm is used to detect the plane surface under the feature [31]. By subtracting the detected plane from the measurement result, a tilt of the sample can be levelled. The position of the laser line on the sample is manipulated along the y-axis, by rotating the mirror around the x-axis. As can be observed in the sectional view, the results of the scanning system shows good agreement with the reference measurement. Only edges (y =-5 mm) can not be detected as sharply, due to the changing incidence angle of the illumination path. In the surface profile some minor differences between the two measurement results are notable. One of them is an artefact around x =0 mm and y =-10 mm in the rotational scan (magenta dashed circle), which is caused by a multiple reflection at a solder joint. This error can also occur at the reference measurement and can be avoided by tilting the sample. Furthermore, it is notable that the plane of the rotational scan is slightly bent (red circle). The reason for this could be, that the Scheimpflug condition is not fulfilled by this setup [32]. The height of a single memory chip is determined to 1.2024 mm with a standard deviation of 40 μm for the SIS and 1.2006 mm with a standard deviation of 37.3 μm for the reference measurement, which emphasizes the good agreement with the reference measurement.

Fig. 8 shows the results of the SIRS compared to the reference measurement. As described earlier, the lateral scan range of the SIRS is smaller, due to the aperture size and the circular mirror shape. Therefore, the measured area is smaller compared to the SIS. In the sectional view, the results of the scanning system correspond even better with reference measurement compared to the results of the SIS. Also in the surface profile there are no differences between the two measurement results notable. Since there is no bending in the surface profile of the SIRS observable, the assumption, that the error in the SIS is caused by the violation of the Scheimpflug condition, is emphasized. The measured

Post-print version of the article: J. Schlarp, E. Csencsics, and G. Schitter, "Optical scanning of laser line sensors for 3D imaging", *Applied optics*, vol. 57, no. 18, pp. 5242–5248, 2018. DOI: 10.1364/AO.57.005242

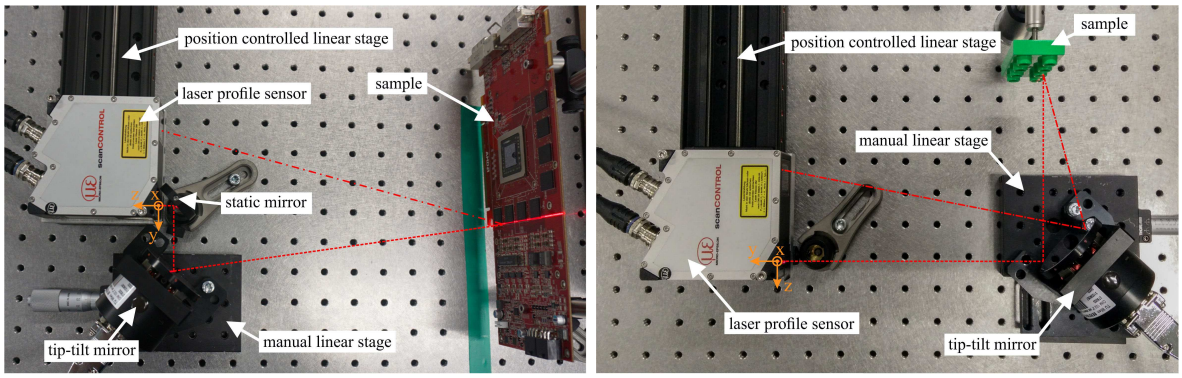

(a) Experimental setup of the SIS (b) Experimental setup of the SIRS

Fig. 6. Experimental setup of the SIS (a) and the SIRS (b). The separate components are arranged according to the ray-tracing simulations. To acquire reference measurements, the laser line sensor is mounted on a position controlled linear stage. Rotational scans are performed at the end position of the controlled stage.

height of a single memory chip is 1.202 mm with a standard deviation of 47 μm, which matches with the reference measurement (1.2006±0.037 mm). The good agreement between the reference measurement and the rotational scan is also observable for the other chosen samples.

In summary, the feasibility of rotational scanning laser line sensors is demonstrated, achieving the same image quality as conventional translational scanning systems and having the advantages of a higher integration level and a lower moving mass for future high speed 3D metrology systems [25].

5. CONCLUSION

In this paper the design and measurement results of two scanning laser line sensors for 3D imaging are shown, demonstrating that rotational scanning of a laser line triangulation sensor is feasible. The architecture of these scanning system is determined with ray-tracing simulations enabling an evaluation of the lateral scan range as well as the accommodated optical path up front. With the geometrical relations, the surface profile of the sample can be reconstructed from the measured dataset. The measurement results show, that the acquired surface profiles of both systems show good agreement with the reference measurement. Therefore, it can be assumed that using a rotational scanning system instead of a conventional translational scanning system does not affect the achievable image quality. Such scanning systems can be better integrated and improve the achievable throughput due to the compact design and lower moving mass respectively. Ongoing work improves the performance of the optical scanning system regarding the scan speed and achievable resolution.

6. FUNDING.

The financial support by the Austrian Federal Ministry for Digital and Economic Affairs and the National Foundation for Research, Technology and Development, as well as MICRO-EPSILON MESSTECHNIK GmbH & Co. KG and ATENSOR Engineering and Technology Systems GmbH is gratefully acknowledged.

REFERENCES

1. R. Schmitt and F. Moenning, "Ensure success with inline-metrology," XVIII IMEKO world congress Metrology for a Sustainable Development (2006).
2. F. Blais, "Review of 20 years of range sensor development," Journal of Electronic Imaging **13** (2004).
3. S. Son, H. Park, and K. H. Lee, "Automated laser scanning system for reverse engineering and inspection," International Journal of Machine Tools & Manufacture **42**, 889–897 (2002).
4. G. Sansoni, M. Trebeschi, and F. Docchio, "State-of-the-art and applications of 3d imaging sensors in industry, cultural heritage, medicine, and criminal investigation," Sensors **9**, 568–601 (2009).
5. H. Schwenke, U. Neuschaefer-Rube, T. Pfeifer, and H. Kunzmann, "Optical methods for dimensional metrology in production engineering," CIRP Annals-Manufacturing Technology **51**, 685–699 (2002).
6. K. Harding, *Handbook of optical dimensional metrology* (CRC Press, 2013).
7. C. P. Keferstein and W. Dutschke, *Fertigungsmesstechnik* (Springer Vieweg, Wiesbaden, 2010).
8. M. Levoy, K. Pulli, B. Curless, S. Rusinkiewicz, D. Koller, L. Pereira, M. Ginzton, S. Anderson, J. Davis, J. Ginsberg, J. Shade, and D. Fulk, "The digital michelangelo project: 3d scanning of large statues," Proceedings of the 27th annual conference on Computer graphics and interactive techniques pp. 131–144 (2000).
9. F. J. Brosed, J. J. Aguilar, D. Guillomía, and J. Santolaria, "3d geometrical inspection of complex geometry parts using a novel laser triangulation sensor and a robot," Sensors **11**, 90–110 (2010).
10. T. Pfeifer, *Koordinatenmeßtechnik für die Qualitätssicherung: Grundlagen—Technologien—Anwendungen—Erfahrungen* (Springer-Verlag, 2013).
11. H. Kunzmann, T. Pfeifer, R. Schmitt, H. Schwenke, and A. Weckenmann, "Productive metrology - adding value to manufacture," CIRP Annals-Manufacturing Technology **54**, 155–168 (2005).
12. R. Leach, *Optical measurement of surface topography*, vol. 14 (Springer, Berlin Heidelberg, 2011).
13. C. Yu, X. Chen, and J. Xi, "Modeling and calibration of a novel one-mirror galvanometric laser scanner," Sensors **17**, 164–178 (2017).
14. Noda, K and Binh-Khiem, N and Takei, Y and Takahata, T and Matsumoto, K and Shimoyama, I, "Multi-axial confocal distance sensor using varifocal liquid lens," 2013 Transducers & Eurosensors XXVII: The 17th International Conference on Solid-State Sensors, Actuators and Microsystems pp. 1499–1502 (2013).
15. W. Boehler and A. Marbs, "3d scanning instruments," Proceedings of the CIPA WG **6**, 9–18 (2002).

Post-print version of the article: J. Schlarp, E. Csencsics, and G. Schitter, "Optical scanning of laser line sensors for 3D imaging", *Applied optics*, vol. 57, no. 18, pp. 5242–5248, 2018. DOI: 10.1364/AO.57.005242

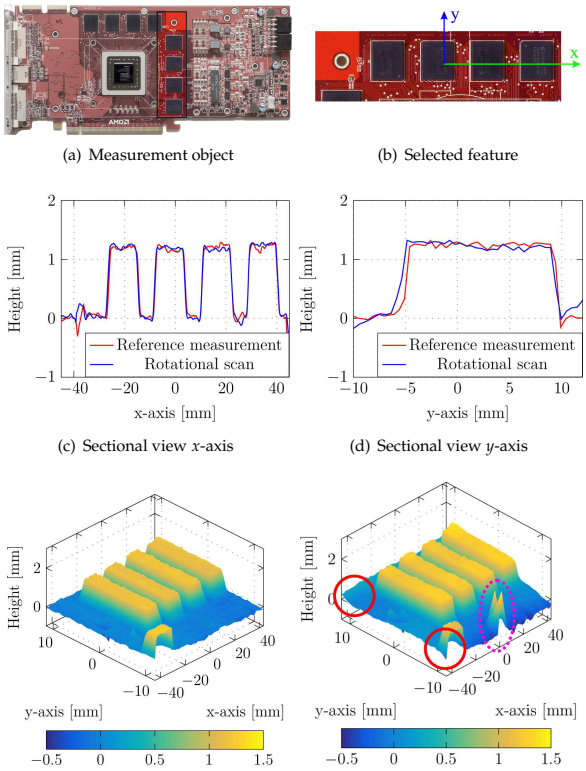

(a) Measurement object (b) Selected feature

(c) Sectional view x-axis (d) Sectional view y-axis

(e) Surface profile reference measurement (f) Surface profile rotational scan

Fig. 7. Comparison between the reference measurement and the measurement with the SIS. The artefact in the rotational scan is caused by a multiple reflection. The plane of the rotational scan is slightly bent (red circle).

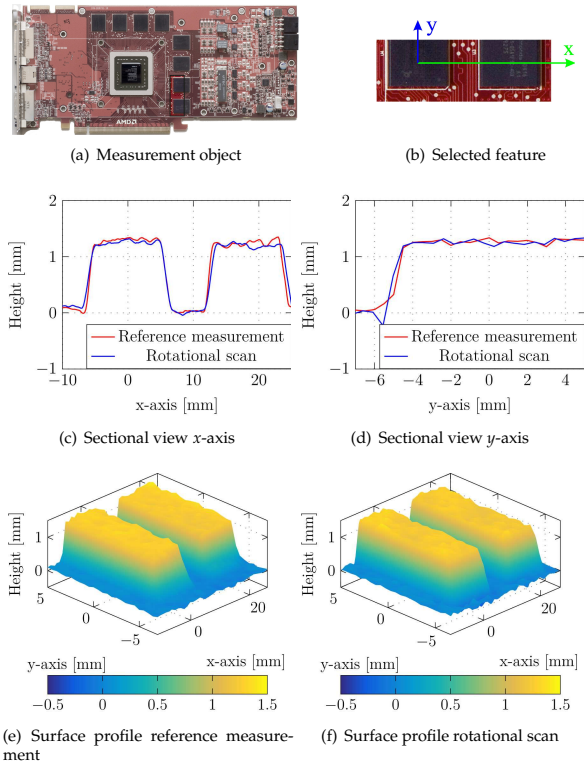

(a) Measurement object (b) Selected feature

(c) Sectional view x-axis (d) Sectional view y-axis

(e) Surface profile reference measurement (f) Surface profile rotational scan

Fig. 8. Comparison between the reference measurement and the SIRS. The results of the rotational scan show good agreement with the reference measurement. Also no bending of the surface in the rotational scan can be observed.

16. W. Boehler, G. Heinz, and A. Marbs, "The potential of non-contact close range laser scanners for cultural heritage recording," International archives of photogrammetry remote sensing and spatial information sciences **34**, 430–436 (2002).
17. Micro-Epsilon Messtechnik GmbH & Co. KG, "Technote - precise non-contact displacement sensors," Tech. Rep. 1 (2014).
18. H. W. Yoo, S. Ito, and G. Schitter, "High speed laser scanning microscopy by iterative learning control of a galvanometer scanner," Control Engineering Practice **50**, 12–21 (2016).
19. R. H. Webb, "Optics for laser rasters," Applied optics **23**, 3680–3683 (1984).
20. S. Xiang, S. Chen, X. Wu, D. Xiao, and X. Zheng, "Study on fast linear scanning for a new laser scanner," Optics & LASER technology **42**, 42–46 (2010).
21. A. Wolter, S.-T. Hsu, H. Schenk, and H. K. Lakner, "Applications and requirements for mems scanner mirrors," in "MOEMS and Miniaturized Systems V," , vol. 5719 (International Society for Optics and Photonics, 2005), vol. 5719, pp. 64–76.
22. M. Hafez, T. Sidler, R. Salathe, G. Jansen, and J. Compter, "Design, simulations and experimental investigations of a compact single mirror tip/tilt laser scanner," Mechatronics **10**, 741–760 (2000).
23. Park, Jung-Ho and Lee, Hu-Seung and Lee, Jae-Hoon and Yun, So-Nam and Ham, Young-Bog and Yun, Dong-Won, "Design of a piezoelectric-driven tilt mirror for a fast laser scanner," Japanese Journal of Applied Physics **51**, 09MD14 (2012).
24. H. F. Mokbel, W. Yuan, L. Q. Ying, C. G. Hua, and A. A. Roshdy, "Research on the mechanical design of two-axis fast steering mirror for optical beam guidance," in "Proceedings of the 1st International Conference on Mechanical Engineering and Material Science," (Atlantis Press, 2012).
25. E. Csencsics, J. Schlarp, and G. Schitter, "High performance hybrid-reluctance-force-based tip/tilt system: Design, control and evaluation," IEEE Transactions on Mechatronics (2018). Accepted.
26. M. Hafez and T. C. Sidler, "Fast-steering two-axis tilt mirror for laser pointing and scanning," in "Microrobotics and Microassembly," , vol. 3834 (International Society for Optics and Photonics, 1999), vol. 3834, pp. 172–182.
27. J. T. Smith, "Elementary euclidean geometry," Methods of Geometry pp. 53–125 (2011).
28. Micro-Epsilon Messtechnik GmbH & Co. KG, *Instruction Manual scanCONTROL 26xx*, Ortenburg (2008).
29. G. F. Franklin, J. D. Powell, and M. L. Workman, *Digital control of dynamic systems*, vol. 3 (Addison-Wesley, Menlo Park, California, 1998).
30. A. Donges and R. Noll, *Laser measurement technology* (Springer, Atlanta, 2015).
31. F. Tarsha-Kurdi, T. Landes, and P. Grussenmeyer, "Hough-transform and extended ransac algorithms for automatic detection of 3d building roof planes from lidar data," in "ISPRS Workshop on Laser Scanning 2007 and SilviLaser 2007," , vol. 36 (2007), vol. 36, pp. 407–412.
32. M. Bass, E. W. Van Stryland, D. R. Williams, and W. L. Wolfe, *Handbook of optics*, vol. 2 (McGraw-Hill, New York, 2001).

Post-print version of the article: J. Schlarp, E. Csencsics, and G. Schitter, "Optical scanning of laser line sensors for 3D imaging", *Applied optics*, vol. 57, no. 18, pp. 5242–5248, 2018. DOI: 10.1364/AO.57.005242